Surface-sandwich segregation and multilayer relaxation on $Pt_{0.5}Ni_{0.5}(110)$ measured by low-energy electron diffraction: An observation of face-related segregation reversal

Y. Gauthier and R. Baudoing
Laboratoire de Spectrométrie Physique, Université Scientifique et Médicale de Grenoble, Boîte Postale 87, 38402 Saint-Martin-d'Hères Cédex, France

M. Lundberg and J. Rundgren
Department of Theoretical Physics, Royal Institute of Technology, S-100 44 Stockholm, Sweden
(Received 18 December 1986)

Low-energy electron diffraction (LEED) is used for measuring the surface segregation and multilayer relaxation on the (110) surface of the $Pt_{0.5}Ni_{0.5}$ alloy. The electron scattering in the substitutionally disordered metallic alloy is described by a layer-by-layer version of the averaged-t-matrix approximation, LEED is calculated by the layer-doubling method (whose convergence is verified), and the measured and calculated spectra are compared by means of metric distances. We find that surface segregation creates a three-layer surface sandwich which has, from the crystal face and inwards, the compositions 100 at. % Ni, 95 at. % Pt, and 83 at. % Ni and the respective multilayer relaxations 19% contraction, 11% expansion, and 1% contraction. The fact that the surface segregation on the (110) face is reversed relative to that which was observed earlier on the (111) face (from the surface and inwards, 88 at. % Pt and 91 at. % Ni) presents a challenge to the theory of alloys. We also discuss the possibility to measure surface vacancy defects by LEED.

I. INTRODUCTION

The present paper reports a low-energy electron diffraction (LEED) investigation of the segregation on $Pt_{0.5}Ni_{0.5}(110)$, which is a random substitutional alloy. LEED was earlier utilized for measuring the segregation on $Pt_xNi_{1-x}(111)$, $x=0.78$, 0.5, and 0.1 (Refs. 1 and 2). The composition profiles found on the mentioned alloy surfaces are depicted in Fig. 1. The surface segregation of $Pt_{0.5}Ni_{0.5}(110)$ is accompanied by multilayer relaxation across three interlayer spacings next to the surface: 19% contraction, 11% expansion, and 1% contraction.

Other recent LEED works on binary alloys concern three ordered alloys, $Cu_3Au(001)$ (Ref. 3), NiAl(110) (Ref. 4), and $Ni_3Al(001)$ (Ref. 5), and one random alloy, $Cu_{0.84}Al_{0.16}(111)$, carrying an ordered overlayer.[6]

Face-related segregation reversal is observed on $Pt_{0.5}Ni_{0.5}$. The outermost layer of the (110) surface is enriched with 100 at.% nickel, while that of the (111) surface is enriched with 88 at. % platinum. The segregation creates such strong compositional oscillation across the outermost layers that the (110) surface can pertinently be described as a three-layer Ni-Pt-Ni sandwich and that the (111) surface can be viewed as a two-layer Pt-Ni sandwich with platinum on top. Work on the segregation on the (100) surface is in progress.

The observation that surface segregation can enrich different species on different crystal faces sheds new light on the previous experimental results on the segregation of polycrystalline platinum-nickel alloys. Earlier either no segregation[7] or a moderate enrichment with platinum[8] was observed. The apparent segregation of a polycrystalline surface will depend on the distribution of crystal faces exposed by the grains.

Theoretically, the segregation of an alloy is driven by a rearrangement of the bonding electron gas, when a semi-infinite crystal is cut away from the infinite bulk material. From the electronic point of view the $Pt_{0.5}Ni_{0.5}$ alloy can be characterized as "a nondilute solution of heavy and light transition metals crystallizing in a fcc lattice with a large atomic-size mismatch." The alloy lattice exhibits 6.6% linear expansion relative to the nickel lattice and 4.3% linear contraction relative to the platinum lattice.[9]

In an imagined pair-bonding picture, the surface segregation is an equilibrium between several interatomic forces: a transition-metal d electron bonding, an attractive (repulsive) strain in the Ni-Ni (Pt-Pt) bonds,[10] and

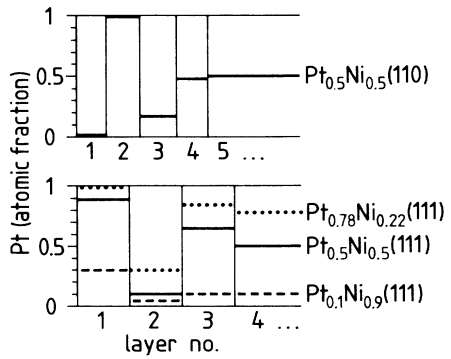

FIG. 1. Segregation on Pt-Ni alloys showing face-related segregation reversal. The composition profile at the (110) surface of $Pt_{0.5}Ni_{0.5}$ (this work) is compared with the composition profiles on the (111) surface of Pt_xNi_{1-x}, $x=0.78$, 0.5, and 0.1 (Refs. 1 and 2).

bond-breaking at the surface.[11] A theoretical approach, where the electronic structure is related to the thermodynamic data for the pure metals or to the electronic density around one metal as an impurity in the other, appears to provide insufficient accuracy for $Pt_{0.5}Ni_{0.5}$.[12–16] A recent theoretical work[17] considering Pt_xNi_{1-x} for all admixtures x takes the atomic size effect into account in a crystal lattice that is kept unrelaxed from the bulk all the way to the surface. In the case of $Pt_{0.5}Ni_{0.5}$ this theory predicts unidirectional segregation in the outermost layer on the (111) and (110) surfaces, 70 at. % and 62 at. % platinum, respectively, while the LEED result is reversed segregation, 88 at. % platinum and 100 at. % nickel.

As shown by the present structure investigation, the alloy lattice is considerably modified by an oscillatory multilayer relaxation near the (110) surface. In a picture allowing for surface relaxation,[18] the interatomic bonding relaxes locally, and one is faced with a self-consistent connection between driving forces, lattice relaxation, and segregation. This interconnection is subtle, as evidenced by the $Pt_{0.5}Ni_{0.5}$ alloy, where platinum is enriched on the (111) face and nickel is enriched on the (110) face.

Segregation is of great technological importance as it can make the surface properties of materials fundamentally different from those of the bulk. The surface-sandwich segregation of $Pt_{0.5}Ni_{0.5}(110)$ may have an interesting physical application. This alloy is nonmagnetic in the bulk, and the question now arises whether sufficient spin coupling would occur among the nickel atoms at the (110) surface for the Ni-Pt-Ni sandwich to exhibit surface magnetism.[19] In chemistry the platinum-nickel alloys serve as catalysts. It is often observed that the catalytic properties are improved, when pure-metal catalysts are alloyed. Such an alloy is $Pt_{0.5}Ni_{0.5}$, whose (111) surface has greater catalytic activity and selectivity with respect to the hydrogenation of butadiene into butenes than the Pt(111) surface.[20] The observation that this alloy is enriched with platinum on the (111) surface and with nickel on the (110) surface may have interesting catalytic implications. The segregation reversal invites one to comparative catalytic studies on the (110) and (111) surfaces of $Pt_{0.5}Ni_{0.5}$ (Ref. 21).

The paper is organized as follows. Section II is experimental and describes the verification of the substitutional disorder in the $Pt_{0.5}Ni_{0.5}(110)$ sample and observations made during the recording of the LEED data. Section III outlines the theoretical plan for the LEED analysis. The electron scattering in a random substitutional alloy is described by means of the averaged-t-matrix approximation, written in a layer-by-layer form suitable for LEED. Possible vacancy defects in the outermost layer can be included in the same calculation. The scattering potentials of platinum (relativistic) and nickel are generated by an excited-state local-density approximation. The scattering is attenuated by atomic vibrations, whose amplitudes are assumed to be enhanced in specific proportions over the three outermost layers. The optimization of a structural model for $Pt_{0.5}Ni_{0.5}(110)$, comprising a multilayer surface segregation and a multilayer relaxation, requires a LEED program that is fast and accurate in the presence of strong scatterers and contracted layer spacings. The matching of theory to experiment is made by the method of metric distances. Section IV is a record of the LEED analysis. A particular study confirmed that electron scattering in the surface sandwich of Fig. 1 is calculable by the layer-doubling method without convergence problems. The multilayer segregation and relaxation illustrated in Fig. 1 is deduced from an excellent agreement between theoretical and experimental spectra for 22 beams recorded both at normal and nonnormal incidence. The uncertainties in the parameter values are estimated by means of the metric distances and are taken proportional to the resolutions derived for the individual parameters. The analysis showed that LEED is capable of measuring a (percentage) density of surface vacancy defects. In Sec. V we discuss the LEED method in relation to other experimental methods for measuring surface segregation, and we compare the LEED results with the current theory of alloys. Section VI is a short summary.

II. EXPERIMENT

A sample of the $Pt_{0.5}Ni_{0.5}(110)$ surface was cut from a rod of single-crystal Pt-Ni alloy having a nominal bulk concentration of 50 at. % platinum.[2] Our x-ray analysis evidences a random substitutional alloy having a fcc lattice with a lattice constant close to the tabulated values 3.749 Å.[9] A (110) section was x-ray oriented and mechanically polished down to a surface roughness of 1 μm. By means of specular reflections produced by an x-ray source and a laser, it was checked that the (110) crystal face was parallel to the polished surface within less than 0.2°.

The surface was cured from defects due to mechanical polishing by 1 h of annealing at about 1300 K, well above the order-disorder transition temperature 918 K.[23] The surface was then cleaned by repeated argon bombardment and annealing up to 1200 K, until the LEED intensities were reproducible. At the latter temperature 2 min of annealing sufficed to yield a sharp diffraction pattern. This is the same procedure as we used in our previous LEED studies of $Pt_xNi_{1-x}(111)$, $x=0.78$, 0.5, and 0.1 (Refs. 1 and 2). The result is an alloy that is frozen in a disordered phase, as confirmed by means of x-ray diffraction before and after the collection of the LEED data.

The LEED apparatus, described elsewhere,[24] allows beam intensities to be measured in the entire half-space above the crystal for any direction of incidence. Normal incidence is defined within 0.1° by means of the crystal-to-ground current at high energy (2 kV); polar angles and azimuths can likewise be set with a precision of 0.1°. The hemispherical grids are interchangeably used for integrated Auger-electron-spectroscopy (AES) measurements to control the surface cleanliness. The residual partial pressure of contaminants is kept low by means of titanium sublimation on a trap cooled at liquid-nitrogen temperature. The basic pressure is of the order of 10^{-10} Torr.

The Pt-Ni sample produced a 1×1 diagram typical of a clean fcc (110) surface. However, under some circumstances, for polar incidence angles larger than 60° and energies larger than 150 eV, we could discern patches and diffuse streaks corresponding to 1×2 and 2×1 domains, but without the well-defined superstructure observed on

Pt(110).[25] We attributed these patches and streaks to partially ordered imperfections and not to impurities, as verified by the Auger spectra. The LEED intensity data were recorded at azimuths for which the aforementioned defects in the diffraction pattern were absent. Owing to the excellent quality of the 1×1 diagram for polar incidence angles smaller than 60°, we concluded that the observed diffraction pattern could be regarded as produced by a 1×1 fcc (110) structure.

At four different incidences we recorded 10, 13, 11, and 12 nonequivalent $I(V)$ spectra in the range 30—250 eV corresponding, respectively, to normal incidence, to the polar angles $\theta=10°$ and 20° with the azimuth $[1\bar{1}0]$, and to the polar angle $\theta=15°$ with the azimuth [001]. The compensating magnetic field of the Helmholtz coils was set so that symmetrically equivalent spots emerged simultaneously and their spectra agreed closely; averaging over symmetrically equivalent beams was not necessary. The spectra were recorded at room temperature by a computer-controlled system in steps of 1 eV. The incident current varied from 10^{-7} A at 30 eV to 10^{-6} A at 200 eV. Reference spectra (incident current, AES, and LEED) were recorded before and after each collection of beam spectra in order to check that no drifting had occurred during the process. After background subtraction, the $I(V)$ curves were normalized to constant incident current.[26]

III. THEORY

A. Disorder, vacancies, and the averaged-t-matrix approximation

The electron bands of a random substitutional alloy are accurately given by the coherent-potential approximation (CPA). Much simpler numerically is the averaged-t-matrix approximation (ATA), which in the cluster method of calculation is the zero-shell approximation of the CPA.[27] LEED from a random substitutional alloy a few rydbergs above the Fermi level appear to be well described by the ATA. The evidence is the previous LEED studies of three Pt-Ni alloys,[1,2] where the agreement between theory and experiment shows similar accuracy as for pure metals with many beams and a large total-energy range.

It is worth noting that there is a specific difference between the use of ATA for the band theory and the application of ATA to surface segregation. In the band theory ATA has the same mix of the species A and B of a random A-B alloy all over the crystal.[27] When ATA is used in a surface structure, the crystal is divided into layers parallel to the surface, and each layer has its particular mix of A and B.[1] The sliced ATA is directly utilizable in a layer-by-layer Korringa-Kohn-Rostoker (KKR) program for LEED calculation.

In the current LEED theory the crystal is assumed to be perfect, but, whatever the care taken in the preparation, the sample is not free of defects like, for instance, vacancies.[28] Within the framework of ATA a vacancy can be regarded as an empty scattering center having vanishing scattering amplitudes:

$$t_{l,\mathrm{vcy}}=0\ , \tag{1}$$

where l indicates partial wave, and vcy is short for vacancy.

Consider, then, a random substitutional A-B alloy divided into layers n parallel to the surface and let $x_A^{(n)}$, $x_B^{(n)}$, and $x_{\mathrm{vcy}}^{(n)}$ be the fractions of atom A, atom B, and vacancies in layer n,

$$x_A^{(n)}+x_B^{(n)}+x_{\mathrm{vcy}}^{(n)}=1\ . \tag{2}$$

The ATA and approximation (1) mimic the electron scattering in an A-B alloy with vacancies by the average scattering amplitudes[1,27]

$$t_l^{(n)}=x_A^{(n)}t_{l,A}+x_B^{(n)}t_{l,B}\ , \tag{3}$$

where $t_{l,A}$ and $t_{l,B}$ are the pure-metal scattering amplitudes of the species A and B.

The simplicity of the ATA formalism invites one to a LEED calculation of a structural model where a concentration of vacancy defects occurs in the outermost layer (Sec. IV C). By LEED one can hope to resolve a vacancy concentration of a few atomic percent.

B. Scattering potential

The scattering amplitudes $t_{l,\mathrm{Pt}}$ and $t_{l,\mathrm{Ni}}$ are conveniently calculated in the following way. The start is the ground-state potential and the electron density for pure platinum and nickel obtained by means of the LMTO (linear muffin-tin orbital) method.[29] Excited-state potentials produced by means of the local-density approximation of Hedin and Lundqvist then give electron-scattering phase shifts corresponding to an energy-dependent inner potential.[30] Platinum is treated relativistically, and the phase shifts are calculated by means of the Pauli equation containing the mass velocity and the Darwin terms. The obtained phase shifts were tested against existing LEED data on clean Pt(111),[31,32] and the agreement was gratifying.

The complex inner potentials for platinum and nickel are approximately the same functions of energy in the range 50—200 eV under consideration. The real, refractive part is calculated from first principles above, and the imaginary, absorptive part is phenomenological and obtained from earlier investigations.[33,34] We are therefore going to use the same complex inner potential $V_R(E)+iV_I(E)$ for all layers of the alloy as in nickel, plus energy-independent real and imaginary shifts $\Delta V_R+i\,\Delta V_I$ to be fitted to the experimental spectra,

$$V_\alpha(E)=V_{\alpha,\mathrm{Ni}}(E)+\Delta V_\alpha,\quad \alpha=R,I\ . \tag{4}$$

The electron absorption due to thermal vibrations is conveniently expressed in terms of the root-mean-square vibrational amplitude u_b in the bulk. Platinum and nickel have such masses and Debye temperatures (240 and 450 K, respectively) that both crystals have approximately the same value of u_b, 0.061 Å, at the ambient temperature 293 K, and we expect that the alloy has a similar value of u_b. Near the surface the atoms vibrate with enhanced amplitudes. Following Clark *et al.*[35] in their calculation of the normal modes of a slab of fcc crystal, we take as vibrational amplitudes in the three outermost layers parallel to the (110) surface

$$u_1 = 1.41u_b,\ u_2 = 1.29u_b,\ u_3 = 1.11u_b\ . \quad (5)$$

u_b is determined from the experimental spectra in the course of the LEED analysis. The relationships (5) give a markedly better approximation than the simplified models, where the vibrational amplitudes are the same through all layers or are enhanced in only the first layer.

C. Structural model

For the (110) surface of fcc metals a considerable amount of information is available concerning the relaxation of the spacing between the first and the second layer: about 10% contraction for Al(110), Ni(110), Cu(110), and Ag(110) (Ref. 33 and references therein), about 15% contraction for Ir(110)-(1×2) (Ref. 36) and Au(110)-(1×2) (Ref. 37), and 20% contraction or possibly 23% expansion in the case of Pt(110)-(1×2) (Ref. 25).

As in our previous work on the segregation of platinum-nickel alloys,[1,2] we design for $Pt_{0.5}Ni_{0.5}(110)$ a structural model composed of a fcc lattice containing layer-wise randomized ATA atoms. The present model employs eight structural parameters: the platinum concentrations in four layers inside the surface, and the interlayer spacings between those four layers (three interlayer relaxations), and, in addition, a concentration of vacancies in the topmost layer. The eight structural parameters are accompanied by another three nonstructural ones as described in the preceding section.

In the following we are going to use a simplified notation for the concentrations: c_n for $x_{\mathrm{Pt}}^{(n)}$, $n=1,2,3,4$, and c_v for $x_{\mathrm{vcy}}^{(1)}$; the relaxations are written Δ_{12}, Δ_{23} and Δ_{34}. We plan to attack the multiparameter LEED problem by steps. Section IV A takes four parameters into account, c_1, c_2, Δ_{12}, and Δ_{23}. Section IV C adds another three parameters, c_3, c_4, and Δ_{34}, and finally allows for c_v.

Many sets of structural parameters have to be scanned by the LEED calculations. With appropriate grids for the eight parameters, one can imagine that of the order of 10^6 beam spectra are to be calculated and compared with the measured spectra. Obviously, even with a vector type of computer, we have to watch the consumption of time. The LEED calculations on the above structural model require both a high speed and a reliable accuracy in the presence of small interlayer spacings and strong scatterers.

D. Computational plan

In the course of this investigation we use two LEED programs, one published by Rundgren and Salwén[38] and another by van Hove and Tong.[39] Both programs have routines based on the layer-doubling method (LDM) for stacking layers, while the latter program is also equipped with the combined-space method (CSM) for forming a composite layer from Bravais-lattice subplanes. The programs give closely agreeing results with parameters for which LDM and CSM are equally valid.

The least interlayer spacing for which the LDM converges is of the order of 1 Å, when strong scatterers occur in the adjacent layers. In the case of the $Pt_{0.5}Ni_{0.5}(110)$ alloy, the convergence of LDM is threatened by the relaxation of the first interlayer spacing, Δ_{12}, which turns out to be a large contraction. We study the convergence of LDM by making comparative calculations by means of the aforementioned LEED programs. The one in Ref. 38 applies LDM all through the surface region of the crystal, while the other in Ref. 39 is used in a version that applies CSM to the two outermost layers and LDM to the crystal underneath. Eight phase shifts are used for the comparative calculations and ten phase shifts in the later production runs by means of LDM (Ref. 38).

The LEED analysis is performed in the range 50–200 eV for theoretical and practical reasons. At low energies ATA is believed to deviate perceptibly from the canonical CPA, and with increasing energy the LEED electrons penetrate deeper into the crystal and get less sensitive to surface segregation.[1] The exclusion of energies below 50 eV avoids the convergence problems of LDM, which are more pronounced at low energies, and a computational stop at 200 eV is required by the time consumption of the CSM program.

For reasons of time we had to content ourselves with matching the multiparameter structural model to 22 experimental spectra, of which ten were recorded at normal incidence and twelve at polar angle 20° along the azimuth $[1\bar{1}0]$. The total length of these recordings is 2530 eV. The LEED patterns from the fcc alloy contain around 30–60 beams at 50–200 eV primary energy, but symmetry reduces the number of beams to 11–19 for normal incidence and to 17–31 for in mirror incidence.

E. Matching theory to experiment

We optimize the structural model by minimizing metric distances between the theoretical and the experimental spectra.[40] A metric distance $D(f,g)$ between two spectra f and g has the strictness property that if $D(f,g)$ tends to zero, it is guaranteed that f approaches g. Strictness is important when an abundance of theoretical spectra are to be compared with a given set of experimental spectra, and visual inspection is impossible except in a few cases. The misfit measure of the least-squares method is the standard example of a metric distance.

We process the spectra using two kinds of normalization and three types of metric distance, D_1, D_2, and D_4 (Ref. 40). The advantage of utilizing several misfit measures is that the spread in the structural parameters gives a hint as to the magnitude of the pertaining uncertainties. The considered metric distances have algorithms that utilize integration and no differentiation and are therefore insensitive to noise and require no smoothing of data. They are themselves fast, and they permit that the LEED calculations are carried out on a time-saving energy grid; in this work we use a 5 eV mesh in the interval 50–200 eV.

Consider two spectra $f(x)$ and $g(x)$ referred to an abscissa $x=(E-E_1)/(E_2-E_1)$ running from 0 to 1 in the given energy range E_1 to E_2. By "normalization to unity" $f(x)$ and $g(x)$ are scaled so that the corresponding primitive functions $F(x)$ and $G(x)$ go from $F(0)=G(0)=0$ to $F(1)=G(1)=1$.

D_1, the strong integrated distance, is an integral over

$|f-g|$. It is similar to but less strong than the least-squares measure, and we use it as a standard reference in all our calculations of metric distances. D_2, the weak integrated distance, is the integral over $|F-G|$. D_4, the Hausdorff distance, is the maximum of the minimum of the radius vector from any point of F to G and, for symmetry, of G to F. For a detailed description of D_1, D_2, and D_4 we refer to previous publications.[33,34,40]

Because of the strictness property the metric distances respond not only to local spectral features due to structural parameters but also, inevitably, to global spectral features connected with nonstructural parameters (as, for instance, the complex inner potential and the mean vibrational amplitude of the atoms). The former parameters we want to study, and the latter ones are now a nuisance. The response to the global features can to some degree be filtered out by renormalization of the theoretical spectra on subintervals.[2] The experimental spectra, being the carriers of true information about the observed phenomenon, are normalized to unity as before.

In addition to D_1, D_2, and D_4, we introduce two misfit measures D_{2p} and D_{4p} based on renormalization. They apply the D_2 and D_4 algorithms combined with "pivot renormalization," where "pivot" refers to a point $x=x_p$ dividing the given energy interval into two subintervals. The theoretical spectrum f is then scaled by one factor on the interval $(0,x_p)$ and by another on the interval $(x_p,1)$, so that the integrated spectrum F takes the same value as G at $x=x_p$. In the present work we choose a pivot situated near the middle of the arc G extending from (0,0) to (1,1) namely, x_p such that $G(x_p)=1-x_p$. Figure 2 illustrates the choice of a pivot and the effect of the renormalization of f by two artificial spectra, whose peaks overlap locally and have different envelopes globally.

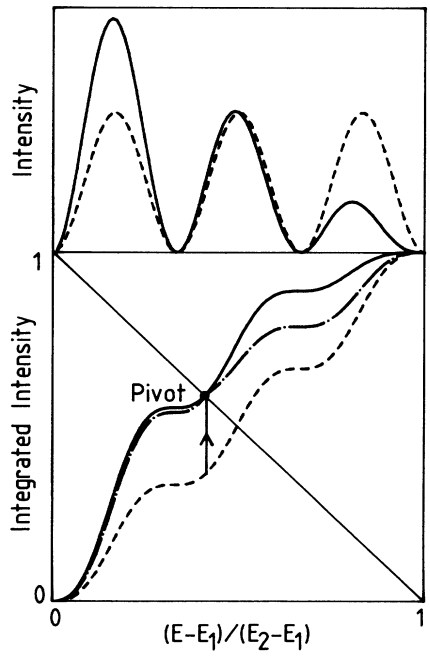

FIG. 2. Renormalization sketched with artifical intensity curves. Current normalization to unity over the interval $E_1<E<E_2$: solid line is experimental and dashed line is theoretical. Renormalization: with separate normalization constants on two intervals, the integrated theoretical curve (dot-dashed line) passes through a pivot on the integrated experimental curve (solid line).

IV. LEED ANALYSIS

A. Search of a surface structure

To search out in an approximate fashion what the surface segregation of $Pt_{0.5}Ni_{0.5}(110)$ is, we design a simplified structural model. We complete the bulk by two fcc (110) layers forming a sandwich having four structural parameters, c_1, c_2, Δ_{12}, and Δ_{23}, together with an inner-potential shift ΔV_R. The grids of the parameters are given as comments to Table I. In the preliminary study we apply the absorptive inner potential of nickel and use a uniform vibrational amplitude 0.061 Å.

We cover every conceivable surface composition by coarse grids of platinum concentrations c_1 and c_2 and choose an extended grid for the relaxation Δ_{12} in the sandwich. The extremes of this grid correspond to the top-layer relaxations discussed for Pt(110)-(1×2).[25] We use a shorter grid of relaxations Δ_{23} below the sandwich, assuming that an alloy has a multilayer relaxation attenuating towards the interior.

The surface structure was explored in a comparative study using two LEED programs (Sec. III D). Metric optimizations against a set of ten nonequivalent experimental spectra recorded at normal incidence gave the lattice relaxation and the composition of material listed in Table I. For this structure the metric distances attain minimum values that are much inferior to the corresponding values anywhere else in the considered parameter space.

The preliminary study shows that $Pt_{0.5}Ni_{0.5}(110)$ segregates with a top layer of almost pure nickel and an underlayer of almost pure platinum. The surface sandwich has

TABLE I. Preliminary model of $Pt_{0.5}Ni_{0.5}(110)$ determined by LEED and metric distances. The optimization is based on ten beam spectra at normal incidence. Notation as in Sec. III.

Metric (%)	c_1[a] (at. %)	c_2[a] (at. %)	Δ_{12}[b] (%)	Δ_{23}[c] (%)	ΔV_R[d] (eV)
$D_1=17.6$	0	91	−20	15	0
$D_2=5.6$	4	100	−20	11	−1
$D_{2p}=2.7$	2	100	−20	13	0
$D_4=10.8$	3	100	−19	12	2
$D_{4p}=6.6$	0	100	−17	10	3
Average	2	98	−19	12	1

[a]The grid $c_1=10(20)90$ at. % combined with the grid $c_2=10(20)90$ at. %, and the grid $c_1=0(10)20$ at. % combined with the grid $c_2=80(10)100$ at. %.
[b]Grid $\Delta_{12}=-30(5)20$ %.
[c]Grid $\Delta_{23}=-10(5)20$ %.
[d]Grid $\Delta V_R=-6(2)6$ eV.

a narrow internal spacing and is separated from the underlying crystal volume by an open spacing as compared with the bulk. This surface sandwich is turned upside down against that occurring on $Pt_{0.5}Ni_{0.5}(111)$,[1] where platinum is strongly enriched in the first layer and much depleted in the second. We thus observe the interesting phenomenon that the segregation of an alloy can reverse from one crystal face to another.

B. LDM convergence

Figure 3 shows that the calculated spectra belonging to the surface structure of Table I agree satisfactorily with the measured ones. Visually the agreement between the two sets of theoretical spectra is good, and the LDM spectra exhibit no sign of a spurious structure in any of the illustrated beams. On these grounds we consider LDM to be convergent for the surface structure under consideration. The metric distance D_1 between the LDM and CSM spectra is 2.0%, which is negligible compared with $D_1 = 17.6\%$ between the calculated and the measured spectra.

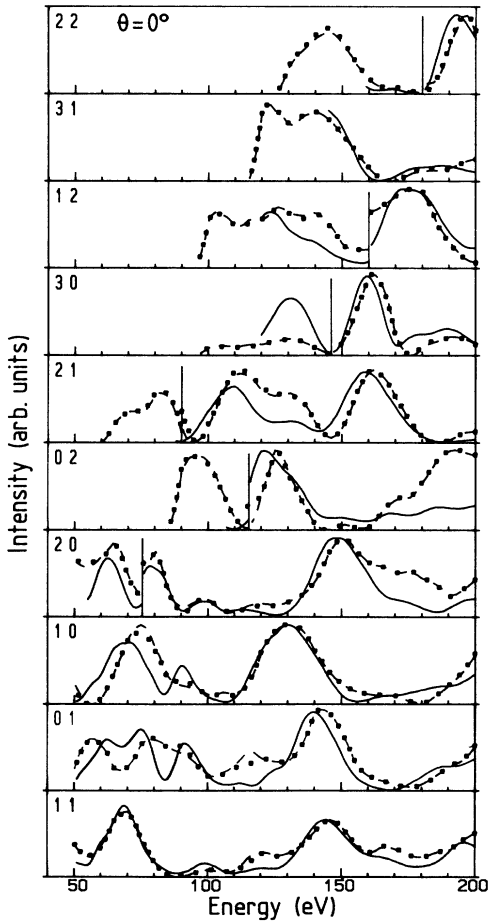

FIG. 3. Beam spectra from $Pt_{0.5}Ni_{0.5}(110)$ interpreted in terms of two-layer segregation and two-layer relaxation. Eight phase shifts are used. Sold line: experiment; dashed line: calculation by CSM; points: calculation by LDM.

We study the convergence of LDM in the (c_1,c_2) space by considering the structural model of the preceding section for parameter values near the optimum ones: $\Delta_{12} = -25\%$, -20%, -15%, $\Delta_{23} = 10\%$, and $\Delta V_R = 0$. The LDM and CSM spectra corresponding to the (c_1,c_2) grids are compared by means of the metric distance D_1. We take the D_1 value 2.5% as a limit of convergence of LDM, which is slightly more tolerant than the D_1 value for the two calculations illustrated in Fig. 3. With this condition LDM proves equivalent to CSM provided that $c_1 + c_2$ is less than or equal to 100 at. % and Δ_{12} is greater than -20%.

Finally we conclude that the use of LDM in the crystal volume below the surface sandwich is justified. Previous evidence on the multilayer relaxation of metals[33] indicates that an alternating and damped bilayer relaxation as obtained in Table I is plausible. In such a case the interlayer spacings from the second one and inwards are greater than or approximately equal to the (110) spacing in the bulk, 1.32 Å, for which LDM is known to work even with layers of pure platinum. In the following a refinement of the structural model is made by LEED calculations based entirely on LDM.

C. Segregation, multilayer relaxation, and vacancy density

In this section we determine the segregation and the multilayer relaxation through four layers of $Pt_{0.5}Ni_{0.5}(110)$. In the LEED calculations we use ten phase shifts for the platinum-nickel scatterers averaged by ATA separately in each layer. For the optimization of the structural model we utilize 22 spectra, of which ten were measured at normal incidence and twelve at 20° incidence along the $[1\bar{1}0]$ azimuth. The agreement between theory and experiment was excellent, and we spent no computing time on the rest of the data base recorded in the experiment (Sec. II).

The optimization of the platinum concentrations follows the iteration scheme in Table II. The final values are obtained by quadratic interpolation separately in each particular concentration. Table III summarizes the results. The multilayer relaxation is represented by fast loops in the LDM type of LEED program, and for each choice of material in the four layers we run 216 multilayer relaxations extending over three interlayer spacings. In the metric optimization these multilayer relaxations are combined with seven shifts of the refractive inner potential. The grids of the last-mentioned parameters are given as comments to Table III.

During the iterations 1—6 we are forced to apply the subsidiary conditions $c_1 > 0$ at. % and $c_2 < 100$ at. % to prevent c_1 and c_2 from gliding towards unphysical values with some metrics, but during the iterations 10—12 we leave the compositional variations free. The resulting negative platinum concentration in the outermost layer, $c_1 = -1$ at. %, is equivalent to zero within the uncertainty of the method. With no restriction on c_1, one is able to assign a standard deviation over metrics to its optimized

value. Iterations 7 and 8 concerning the vibrational amplitudes of the alloy substantially diminish the metric distances and clearly favor the thermal model having enhanced amplitudes in three layers as given by expressions (5). Iteration 9 shows that the absorptive potential of the alloy closely agrees with that of pure nickel.

The result of the LEED analysis is given by the last three lines of Table III. The structural parameters are averages over metrics, and the standard deviations are those which follow from the spread among the metric distances. The uncertainties given are estimated from considerations of resolution in Sec. IV D. Figure 4 shows the LEED spectra belonging to the optimized surface structure. The values of the metric distances are remarkably low, in fact, lower than the ones obtained in a previous work on Ni(110).[33]

The surface segregation of $Pt_{0.5}Ni_{0.5}(110)$ is found to take place in three layers, containing, from the surface and inwards, pure nickel, $c_1 = 0$ at. %, almost pure platinum, $c_2 = 95$ at. %, and a high fraction of nickel, $c_3 = 17$ at. %. The composition of the fourth layer, $c_4 = 48$ at. %, is similar to that of the bulk. The multilayer relaxation turns out to be alternating, beginning with a large contraction at the surface. This behavior is similar to the multilayer relaxation established for the (110) surface of a number of pure metals.[33]

An optimization of the vacancy density in the outermost layer gives 3 at. %. From arguments of resolution and standard deviations over metrics the uncertainty in this value is estimated to be 7 at. %.

TABLE II. Optimization of the composition profile of $Pt_{0.5}Ni_{0.5}(110)$. Parameter grids and optimum values are given for each iteration. Intervals $a-b$ show the spread in optimum values resulting from five metrics. Notation as in Sec. III.

Iteration	c_1	c_2	c_3	c_4	ΔV_I	u_b
	(at. %)				(eV)	(10^{-2} Å)
1 grid	0(10)20	80(10)100	50	50	0	6.1[a]
opt.	0—5	90—100				
2 grid	0	100	0(10)50	50	0	6.1[a]
opt.			0—20			
3 grid	10	100	0(10)30	50	0	6.1[a]
opt.			0—20			
4 grid	0	90	0(10)30	50	0	6.1[a]
opt.			0—20			
5 grid	0(5)10	90(5)100	20	50	0	6.1[a]
opt.	Table III	Table III				
6 grid	0	100	0(10)20	30(20)70	0	6.1[a]
opt.			Table III	Table III		
7 grid	0	100	20	50	0	5.4(0.7)6.8[b]
opt.						5.8—6.1
8 grid	0	100	20	50	0	5.4(0.7)6.8[c]
opt.						Table III
9 grid	0	100	20	50	−0.6(0.6)0.6	6.1[c]
opt.					Table III	
10 grid	−10(5)10	85(5)100	20	50	0	6.1[c]
opt	Table III	Table III				
11 grid	0	95	0(10)30	50	0	6.1[c]
opt.			Table III			
12 grid	0	95	20	30(20)70	0	6.1[c]
opt.				Table III		

[a]The same value in all layers.
[b]Enhanced value in the first layer, $u_1 = 1.41u_b$.
[c]Enhanced values in three layers, $u_1 = 1.41u_b$, $u_2 = 1.29u_b$, $u_3 = 1.11u_b$.

D. Resolution

In an attempt to estimate the uncertainty in the optimizations of Table III we study the resolution of the LEED machinery (given experimental data, LEED program, and metric program) with respect to the structural parameters. We discuss ten structural parameters p_i, each of which takes values on a grid of mesh m_i and has an optimum value p_i^{opt}. The correspondence with the notation of the preceding sections is

$$\mathbf{p}=(c_1,c_2,c_3,c_4\Delta_{12},\Delta_{23},\Delta_{34},\Delta V_R,\Delta V_I,u_b)\ . \tag{6}$$

A metric distance D_n, $n=1,2,4,2p,4p$, used in the structural optimization is a function of p_i and attains its minimum D_n^{opt} for $p_i=p_i^{\text{opt}}$. The LEED calculations show that D_n is to a good approximation a parabola with respect to each parameter varied separately through the optimum,

$$D_n=k_i[(p_i-p_i^{\text{opt}})/m_i]^2+D_n^{\text{opt}}\ . \tag{7}$$

In the case of D_1, D_2, and D_4, we have to refer the parabola of $p_1=c_1$ to a virtual p_1^{opt} value which is a few percent negative (Table III).

With properly dimensioned meshes m_i, one has $k_i=k$, and all the parabolas are identical in the variables $(p_i-p_i^{\text{opt}})/m_i$. In such a case the meshes m_i form a set of isoresolution meshes: A displacement of any parameter p_i by one mesh from the optimum, while the other parameters are kept fixed at the optimum, will give equal metric response from the LEED machinery.

Table IV gives the crude meshes on which the LEED calculations were carried out, together with the isoresolution meshes derived for each metric distance after the optimization. When the isoresolution meshes are normalized, for instance, to $m_5=1\%$, all the meshes m_i are seen to be roughly uniform over metrics.

As uncertainty in an optimized structural parameter we propose

$$\Delta p_i=m_i \max_k \{s_k/m_k\}\ , \tag{8}$$

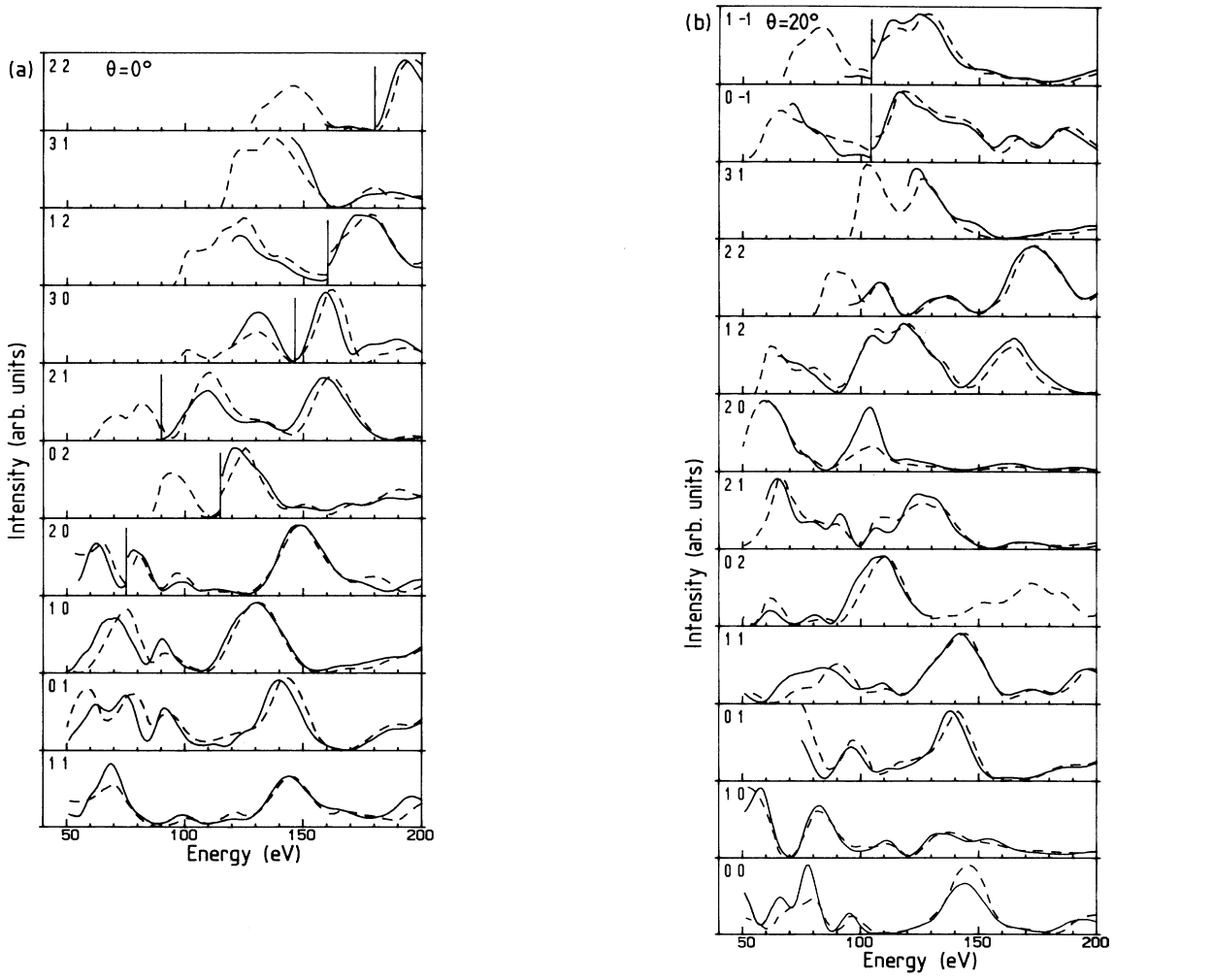

FIG. 4. Beam spectra from $Pt_{0.5}Ni_{0.5}(110)$ interpreted in terms of four-layer segregation and three-layer relaxation. Ten phase shifts are used. (a) Normal incidence and (b) incidence 20° from normal in the $[1\bar{1}0]$ azimuth. Solid line, experiment; dashed line, calculation.

TABLE III. Surface segregation and multilayer relaxation on $Pt_{0.5}Ni_{0.5}(110)$ determined by metric optimization on 22 LEED spectra at normal and off-normal incidence. Averages and standard deviations refer to metrics; the uncertainties follow from standard deviations and isoresolution meshes. Notation as in Sec. III.

Metric (%)	c_1	c_2 (at. %)	c_3	c_4	Δ_{12}[a]	Δ_{23}[b] (%)	Δ_{34}[c]	ΔV_R[d] (eV)	ΔV_I	u_b (10^{-2} A)
					Iterations 5 and 6 in Table II					
$D_1=11.3$	0	100	18	50	−18.9	10.4	−0.8	−1.3	0	6.1[e]
$D_2=3.4$	0	100	0	27	−19.8	10.3	−2.4	−3.0	0	6.1[e]
$D_{2p}=1.8$	1	100	12	50	−19.0	9.9	0.1	−2.0	0	6.1[e]
$D_4=6.8$	8	100	10	15	−19.0	9.4	−1.4	−0.1	0	6.1[e]
$D_{4p}=4.3$	1	97	11	5	−19.2	9.9	−0.2	−0.9	0	6.1[e]
					Iterations 8 to 12 in Table II					
$D_1=9.8$	−2	94	21	50	−19.0	10.0	−1.0	−1.0	0.0	5.8[f]
$D_2=2.3$	−5	95	11	46	−18.9	10.3	−1.7	−1.1	0.2	5.9[f]
$D_{2p}=1.5$	2	99	19	48	−18.9	10.1	0.1	−0.1	−0.1	6.2[f]
$D_4=5.0$	−2	89	13	48	−19.7	11.4	−2.6	−1.1	0.4	6.0[f]
$D_{4p}=3.8$	2	97	19	48	−18.8	10.6	0.5	−0.5	−0.8	6.0[f]
					Result					
Average	−1	95	17	48	−19.2	10.5	−0.9	−1.0	−0.1	6.0
Standard deviation	3	4	4	1	0.4	0.5	1	0.5	0.5	0.1
Uncertainty	6	4	7	13	0.6	1.0	1.4	0.7	0.7	0.6

[a]Grid $\Delta_{12}=-21(1)-16$ %.
[b]Grid $\Delta_{23}=7.5(1.25)13.75$ %.
[c]Grid $\Delta_{34}=-5.33(1.33)1.33$ %.
[d]Grid $\Delta V_R=-4(1)1$ eV.
[e]The same value in all layers.
[f]Enhanced value in three layers, $u_1=1.41u_b$, $u_2=1.29u_b$, $u_3=1.11u_b$.

where s_i is the standard deviation with respect to the metrics (Table III) and m_i is the isoresolution mesh (Table IV). The estimate (8) yields the least uncertainties that are proportional to the isoresolution meshes and enclose all the standard deviations. The resulting uncertainties are listed at the bottom of Table III. Our estimate is based on the hypothesis that the five metrics together examine all significant spectral features. Other prescriptions for searching a general level of uncertainty of LEED analyses use the the count of peaks in the spectra.[41,42]

TABLE IV. Isoresolution meshes with respect to metric distance. First line: the crude meshes used in Table III; last line: averages over metrics. Notation as in Sec. III.

	Mesh of parameter									
Type of mesh	c_1 m_1	c_2 m_2 (at. %)	c_3 m_3	c_4 m_4	Δ_{12} m_5	Δ_{23} m_6 (%)	Δ_{34} m_7	ΔV_R m_8 (eV)	ΔV_I m_9	u_b m_{10} (10^{-2} Å)
Crude	5	5	10	20	1	1.25	1.33	1.0	0.6	0.7
D_1	9	8	13	19	1	1.4	2.2	1.0	1.2	1.4
D_2	9	8	14	24	1	2.1	2.5	1.5	1.0	0.8
D_{2p}	10	7	16	24	1	2.0	2.1	1.4	1.1	1.5
D_4	7	6	14	26	1	1.9	3.1	1.7	1.2	0.7
D_{4p}	6	6	9	19	1	1.2	2.4	1.0	1.4	1.2
Isoresolution[a]	8	7	13	22	1	1.7	2.5	1.3	1.2	1.1

[a]With normalization to $m_5=1$%. A normalization to $m_2=4$ at. % through expression (8) gives the uncertainties on the bottom line of Table III.

V. DISCUSSION

A. On the LEED result

Up till now LEED has been utilized for measuring the surface segregation on four random bimetallic alloys, namely $Pt_xNi_{1-x}(hkl)$ for $x=0.78,0.1$, $hkl=111$ and $x=0.5$, $hkl=111,110$ (Refs. 1 and 2 and this work). A general conclusion is that LEED is capable of resolving the in-depth composition of a random bimetallic alloy through three layers on a close-packed surface and through four layers on an open surface, provided that the metals have large and different electron-scattering cross sections. The promise of LEED as a method for measuring surface segregation is discussed in the Introduction to Ref. 1 in relation to other methods: Auger-electron spectroscopy (AES), x-ray photoelectron spectroscopy (XPS), ion-scattering spectroscopy (ISS), and time-of-flight field-ion spectroscopy. For three $Pt_xNi_{1-x}(111)$ alloys the composition of the outermost layer comes out the same as by AES and ISS for $x=0.78$ and 0.5 (Refs. 1 and 43), and as by AES, XPS, and ISS for $x=0.1$ (Refs. 2 and 44).

That ATA is indeed sufficiently accurate to produce as small uncertainties as those found in Table III is indicated by the aformentioned agreement between LEED and other methods and by the manifestly good numerical description of hitherto 95 spectra extending over a total range of 11 000 eV. A direct comparison between ATA and CPA, which is the canonical method for describing random metallic alloys, is available for energies up to and including the Fermi level.[29] A similar direct ATA study for a LEED situation involving energies up to 200 eV and angular momenta up to $l=9$ would be elucidating but is outside the scope of this paper.

The conservation relation (2) imposes a useful numerical condition on the optimization procedure. In the mathematical analysis the atomic fractions can be varied on grids extending inside and outside the interval 0—100 at. %, but it is a necessary physical condition that the optimization procedure yields values inside that range. With reference to the parabolic behavior of the metric distances around the minimum as given by expression (7), we assign a symmetric plus-minus uncertainty to any composition, including the end points of the physical interval 0—100 at. %. In the present investigation c_1 is varied below 0 at. % and c_2 above 100 at. %, and the issue, $c_1=-1\pm6$ at. % and $c_2=95\pm4$ at. %, is acceptable under the above conditions; the value of c_1 is indistinguishable from $c_1=0^{+5}_{-0}$ at. %.

Surface vacancies are considered in this paper on surface segregation for three reasons. They are one conceivable cause of a diffuse background to the diffraction pattern, and theoretically they are easily included in the layerwise ATA model for segregation. Besides, a vacancy density imposes an additional condition on the optimization procedure in that it lies in the 0—100 at. % range, and often at the very low end. The conservation relation (2) for the outermost layer is a sensitive balance between two atomic fractions and one vacancy fraction. The present value of the latter, $c_v=3^{+7}_{-3}$ at. %, is acceptable on the above grounds.

The possible occurrence of 3 at. % vacancy defects on $Pt_{0.5}Ni_{0.5}(110)$ can be compared with the 1×2 reconstruction of pure Pt(110),[25] which corresponds to 50 at. % ordered vacancies. There is a correlation between the vacancy density c_v and the enhancement factor u_1/u_b of the thermal vibrations which both weaken the coherent backscattering from the outermost layer, but this correlation is not studied in detail here. Nevertheless, the present work shows that it is thinkable to gain quantitative information from LEED spectra on random vacancy defects, a structural problem for which very few techniques are available.[28] Wanted now is a scanning tunneling microscopy image, where the platinum atoms, the nickel atoms, and possible vacancy defects in the outermost layer can be counted in real space.

A remark is in order concerning the definition of the multilayer relaxation. In Table III the reference structure is the bulk of $Pt_{0.5}Ni_{0.5}$, whose lattice constant is 3.749 Å (standard 1). Another imaginable standard is a $Pt_{0.5}Ni_{0.5}(110)$ structure having the near-surface composition of Table III and interlayer separations given by hard-sphere radii taken from Pearson's handbook[9] for the layer composition of each particular layer (standard 2). Geometrically, standard 2 exhibits, from the first layer and inwards, 4.3% contraction and 0.4% expansion relative to standard 1. These relaxations derive from the compositions c_1, c_2, and c_3, which have moderate uncertainties. One can say that the large contraction given in Table III for the outermost layer, 19.2%, stems from one contraction, 4.3%, that is geometrical and another, 14.9%, that is due to surface relaxation of the interatomic forces.

B. On the theory of alloys

Particularly interesting for the use of platinum-nickel alloys in physics and chemistry is the result that the surface segregation enriches 88 at. % platinum on the close-packed (111) surface and, reversely, enriches 100 at. % nickel on the open (110) surface. Comparison with the result of the previous measurements on polycrystalline platinum-nickel samples[7,8] is not possible, since the reversed segregations, observed on two low-index surfaces so far, average out in a powder of crystallites. Likewise, previous empirical theory based on polycrystalline concepts[12–14] becomes inapplicable to cases where segregation reversal occurs. Near the surface the interatomic forces vary with the depth, and several attempts have been made to take this variation into account through pair-bonding models. Williams and Nason[15] introduce surface-bond enthalpies which are relaxed in relation to the bulk bond enthalpies. King and Donnelly[11] refine the idea to an *a priori* calculation of the bond enthalpy relaxations from pure-metal data on the heat of sublimation, the energy of bulk vacancy formation, and the surface energy.

Explaining the face-related segregation reversal on $Pt_{0.5}Ni_{0.5}$ is a challenge to the theory of alloys. Tomanek *et al.*[16] discuss segregation reversal in connection with an electronic theory for impurity segregation at metal surfaces. In the theory, a rhenium impurity in platinum has

a small heat of segregation that changes sign from one crystal face to another which leads to the prediction that dilute rhenium is depleted by a factor of 0.7 on Pt(Rh)(111) and enriched by a factor of 1.02 on Pt(Rh)(110) (at 1000 K). Tréglia and Legrand[17] consider two fcc binary alloys over the entire concentration interval, assuming an unrelaxed semi-infinite lattice and using a tight-binding approach for a calculation of the atomic-size effect. For $Pt_{0.5}Ni_{0.5}$(111) their theory gives an oscillatory composition profile in the three outermost layers in qualitative agreement with the LEED measurement, namely, 70, 43, and 52 at. % platinum,[17] relative to 88, 9, and 65 at. % platinum.[1] In the case of $Pt_{0.5}Ni_{0.5}$(110) the same theory suggests a composition profile that proves dissimilar to the LEED result, namely, 60, 62, and 39 at. % platinum[17] against 0, 95, and 17 at. % platinum (this work), which leaves the measured segregation reversal unexplained.

Required for the study of segregation reversal is a coherent-potential theory that, firstly, is valid for any admixture of one metal in the other and, secondly, is capable of interconnecting the segregation on an open surface with a multilayer relaxation of the lattice. Simultaneous surface segregation and lattice relaxation can be taken into account by means of statistical mechanics and Monte Carlo simulation. Foiles[18] applies this method to three low-index surfaces of nickel-copper alloy, however, without reporting any relaxation of the surface layers.

VI. SUMMARY

In this paper we report a LEED investigation of the segregation on the (110) surface of the $Pt_{0.5}Ni_{0.5}$ alloy. Upon annealing the sample at 1300 K, 400° above the order-disorder temperature, the surface exhibited a 1×1 fcc (110) LEED pattern. X-ray analysis before and after the LEED recordings showed that the bulk composition remained substitutionally disordered. The presented LEED analysis follows a theoretical plan that comprises layerwise ATA for describing the electron scattering in a segregated metallic alloy, LEED calculations by means of a layer-doubling program, and structural optimization based on metric distances between spectra.

We find that the segregation on the $Pt_{0.5}Ni_{0.5}$(110) alloy creates a surface sandwich, which in three layers from the surface and inwards contains enrichments of 100 at. % Ni, 95 at. % Pt, and 83 at. % Ni. The surface segregation is accompanied by a substantial multilayer relaxation relative to the (110) spacing in the bulk, 1.325 Å, namely, 19% contraction, 11% expansion, and 1% contraction, In an explorative calculation we obtained a 3 at. % density of vacancy defects in the outermost layer. The structural parameters together with the pertaining uncertainties are given below, where c_i is the platinum content of the ith layer, c_v is the density of vacancy defects in the outermost layer, and d_{ii+1} is the spacing between the ith and the $(i+1)$th layer:

$$c_1 = 0^{+5}_{-0} \text{ at. \% and } c_v = 3^{+7}_{-3} \text{ at. \%},$$

$$c_2 = 95\pm4 \text{ at. \%},$$

$$c_3 = 17\pm7 \text{ at. \%},$$

$$c_4 = 48\pm13 \text{ at. \%},$$

$$d_{12} = 1.07\pm0.01 \text{ Å},$$

$$d_{23} = 1.47\pm0.02 \text{ Å},$$

$$d_{34} = 1.31\pm0.02 \text{ Å}.$$

The surface sandwich segregation on the (110) face is to be compared with its counterpart on the (111) face, where the composition is 88, 9, and 65 at. % platinum in three layers from the surface and inwards.[1] Spectacular from the theoretical point of view is that the segregation reverses from the (110) face to the (111) face and enriches, most efficiently, nickel on one face and platinum on the other. The segregation reversal is an interesting phenomenon which can hopefully be exploited in studies of catalytic and magnetic surface effects.

ACKNOWLEDGEMENTS

The work performed at Grenoble is supported by Centre National de la Recherche Scientifique, under the scientific program of the Groupement Surfaces Rhône-Alpes, and by the scientific council of Centre de Calcul Vectoriel pour le Recherche (Palaiseau, France). Laboratoire de Spectrométrie Physique (Saint-Martin-d'Hères, France) is "Laboratoire associé au Centre National de la Recherche Scientifique." The work performed at Stockholm is supported by the Swedish Natural Science Research Council (NFR) and by the Cray-1 Committee of NFR. We are indebted to G. Rolland for his assistance on the x-ray part of the sample preparation.

[1] Y. Gauthier, Y. Joly, R. Baudoing, and J. Rundgren, Phys. Rev. B **31**, 6216 (1985).
[2] R. Baudoing, Y. Gauthier, M. Lundberg, and J. Rundgren, J. Phys. C **19**, 2825 (1986).
[3] T. M. Buck, G. H. Wheatley, and L. Marchut, Phys. Rev. Lett. **51**, 43 (1983).
[4] H. L. Davis and J. R. Noonan, Phys. Rev. Lett. **54**, 566 (1985); J. R. Noonan and H. L. Davis, Science **234**, 310 (1986).
[5] D. Sondericker, F. Jona, and P. M. Marcus, Phys. Rev. B **33**, 900 (1986).
[6] R. J. Baird, D. F. Ogletree, M. A. Van Hove, and G. A. Somorjai, Surf. Sci. **165**, 345 (1986).
[7] J. J. Burton and R. S. Polizzotti, Surf. Sci. **66**, 1 (1977).
[8] J. Sedlacek, L. Hilaire, P. Legare, and G. Maire, Surf. Sci. **115**, 541 (1982); Appl. Surf. Sci. **10**, 75 (1982).
[9] W. B. Pearson, *A Handbook of Lattice Spacings and Structures of Metals and Alloys* (Pergamon, London, 1964).
[10] A. D. van Langeveld and A. J. Staverman, Z. Metallk. **76**, 54 (1985).
[11] T. S. King and R. G. Donnelly, Surf. Sci. **141**, 417 (1984), and references therein.
[12] A. R. Miedema, Z. Metallk. **69**, 455 (1978).
[13] J. R. Chelikovsky, Surf. Sci. **139**, L197 (1984).
[14] F. F. Abraham and C. R. Brundle, J. Vac. Sci. Technol. **18**,

506 (1981).
[15]F. L. Williams and D. Nason, Surf. Sci. **45**, 377 (1974); M. S. Spencer, *ibid.* **145**, 153 (1984).
[16]D. Tomanek, A. A. Aligia, and C. A. Baliseiro, Phys. Rev. B **32**, 5051 (1985).
[17]G. Tréglia and B. Legrand, Phys. Rev. B **35**, 4338 (1987).
[18]S. M. Foiles, Phys. Rev. B **32**, 7685 (1985); S. M. Foiles, M. I. Baskes, and M. S. Daw, *ibid.* **33**, 7983 (1986).
[19]J. Kirschner (private communication).
[20]J. Massardier and J. C. Bertolini, J. Catal. **90**, 358 (1984); Y. Gauthier, R. Baudoing, Y. Joly, J. Rundgren, J. C. Bertolini, and J. Massardier, Surf. Sci. **162**, 342 (1985).
[21]J. C. Bertolini (private communication).
[22]Purchased from Cristal Tec, Centre d'Etudes Nucléaires de Grenoble (CENG), 38041 Grenoble, France.
[23]R. Hultgren, P. D. Desai, D. T. Hawkins, M. Gleiser, and K. K. Kelley, *Selected Values of the Thermodynamic Properties of Binary Alloys* (American Society for Metals, Metals Park, Ohio, 1973).
[24]L. de Bersuder, Rev. Sci. Instrum. **45**, 1569 (1974).
[25]D. L. Adams, H. B. Nielsen, M. A. Van Hove, and A. Ignatiev, Surf. Sci. **104**, 47 (1981).
[26]The digitized data are available from the authors upon request.
[27]B. L. Györffy and G. M. Stocks, in *Electrons in Disordered Metals and at Metallic Surfaces,* edited by P. Phariseau, B. L. Györffy, and L. Scheire (Plenum, New York, 1979), p. 89.
[28]J. M. Blakely and M. Eizenberg, in *The Chemical Physics of Solid Surfaces and Heterogeneous Catalysis,* edited by D. A. King and D. P. Woodruff (Elsevier, Amsterdam, 1981), Vol. 1, p. 1.
[29]O. K. Andersen, Phys. Rev. B **12**, 3060 (1975).
[30]R. E. Watson, J. F. Herbst, L. Hodges, B. I. Lundqvist, and J. W. Wilkins, Phys. Rev. B **13**, 1463 (1976); J. Neve, J. Rundgren, and P. Westrin, J. Phys. C **15**, 4391 (1982); J. Neve, P. Westrin, and J. Rundgren *ibid.* **16**, 1291 (1983).
[31]D. L. Adams, H. B. Nielsen, and M. A. Van Hove, Phys. Rev. B **20**, 4789 (1979).
[32]Y. Gauthier and R. Baudoing (unpublished).
[33]Y. Gauthier, R. Baudoing, Y. Joly, C. Gaubert, and J. Rundgren, J. Phys. C **17**, 4547 (1984).
[34]S. A. Lindgren, L. Walldén, J. Rundgren, and P. Westrin, Phys. Rev. B **29**, 576 (1984).
[35]B. C. Clark, R. Herman, and R. F. Wallis, Phys. Rev. **139**, A860 (1965).
[36]C. M. Chan, M. A. Van Hove, W. H. Weinberg, and E. D. Williams, Surf. Sci. **91**, 440 (1980).
[37]W. Moritz and D. Wolf, Surf. Sci. **88**, L29 (1979).
[38]J. Rundgren and A. Salwén, J. Phys. C **9**, 3701 (1976).
[39]M. A. Van Hove and S. Y. Tong, *Surface Crystallography by LEED* (Springer, Berlin, 1979).
[40]J. Philip and J. Rundgren, in *Determination of Surface Structure by LEED,* edited by P. M. Marcus and F. Jona (Plenum, New York, 1984), p. 409.
[41]J. B. Pendry, J. Phys. C **13**, 937 (1980).
[42]J. N. Andersen, H. B. Nielsen, L. Petersen, and D. L. Adams, J. Phys. C **17**, 173 (1984).
[43]L. De Temmerman, C. Creemers, H. Van Hove, A. Neyens, P. Delichere, J. Massardier, B. Tardy, M. Abon, and J. C. Bertolini, Vide Couches Minces **38**, 217 (1983).
[44]J. C. Bertolini, J. Massardier, P. Delichere, B. Tardy, B. Imelik, Y. Jugnet, Tran Min Duc, L. De Temmerman, C. Creemers, H. Van Hove, and A. Neyens, Surf. Sci. **119**, 95 (1982).